

UCSF

UC San Francisco Previously Published Works

Title

Separation of extracellular nanovesicles and apoptotic bodies from cancer cell culture broth using tunable microfluidic systems

Permalink

<https://escholarship.org/uc/item/38h5q90d>

Journal

Scientific Reports, 7(1)

ISSN

2045-2322

Authors

Shin, Soojeong
Han, Daeyoung
Park, Min Chul
et al.

Publication Date

2017

DOI

10.1038/s41598-017-08826-w

Peer reviewed

SCIENTIFIC REPORTS



OPEN

Separation of extracellular nanovesicles and apoptotic bodies from cancer cell culture broth using tunable microfluidic systems

Soojeong Shin¹, Daeyoung Han^{2,3}, Min Chul Park^{2,4}, Ji Young Mun^{5,6}, Jonghoon Choi⁷, Honggu Chun⁸, Sunghoon Kim^{2,3} & Jong Wook Hong^{1,9}

Extracellular vesicles (EVs) are the cell-secreted nano- and micro-sized particles consisted of lipid bilayer containing nucleic acids and proteins for diagnosis and therapeutic applications. The inherent complexity of EVs is a source of heterogeneity in various potential applications of the biological nanovesicles including analysis. To diminish heterogeneity, EV should be isolated and separated according to their sizes and cargos. However, current technologies do not meet the requirements. We showed noninvasive and precise separation of EVs based on their sizes without any recognizable damages. We separated atto-liter volumes of biological nanoparticles through operation of the present system showing relatively large volume of sample treatment to milliliters within an hour. We observed distinct size and morphological differences of 30 to 100 nm of exosomes and apoptotic bodies through TEM analysis. Indeed, we confirmed the biological moiety variations through immunoblotting with noninvasively separated EVs opening new windows in study and application of the biological nanoparticles.

The complexity of a biological system can be resolved by using its physicochemical properties to isolate and separate its specific constituent bio-organisms and -molecules, such as cells, bacteria, proteins, and DNA. Recently, there is an emerging need to isolate and separate extracellular vesicles (EVs). EVs are lipid bilayer vesicles secreted by cells, and generally, the size ranges between hundreds of nanometers. Since EVs contain specific biomolecules such as protein, mRNA, and microRNA, their potential application in diagnostics and therapeutics^{1–3} has garnered considerable attention.

Besides the size and density, EVs' heterogeneity also derives from the diverse cargo inserted in EVs, making it arduous for researchers to determine their exact functions⁴. Based on accumulated evidence, EVs are classified into exosomes, microvesicles, and apoptotic bodies⁴. Of these, exosomes, a well-characterized EV type, are of particular interest to the medical and pharmaceutical fields⁵. Exosomes are membranous vesicles of endosomal origin with 50–200 nm hydrodynamic diameter and have biologically significant molecules⁶.

However, a validated protocol for the isolation of these small vesicles with diameters of approximately 100 nm has not been suggested yet. The most commonly used method is ultracentrifugation, which is time and energy consuming, and has the risk of introducing protein and other types of EV contamination because of a highly

¹Department of Bionano Engineering, Hanyang University, Ansan, 15588, Korea. ²Medicinal Bioconvergence Research Center, Seoul National University, Seoul, 08826, Korea. ³Department of Molecular Medicine and Biopharmaceutical Sciences, Graduate School of Convergence Technology, College of Pharmacy, Seoul National University, Seoul, 08826, Korea. ⁴Advanced Institutes of Convergence Technology, Seoul National University, Suwon, 16229, Korea. ⁵Department of Biomedical Laboratory Science, College of Health Sciences, Eulji University, Seongnam, 13135, Korea. ⁶BK21 Plus Program, Department of Senior Healthcare, Graduate School, Eulji University, Daejeon, 34824, Korea. ⁷School of Integrative Engineering, Chung-Ang University, Seoul, 06974, Korea. ⁸Department of Biomedical Engineering, Korea University, Seoul, 02841, Korea. ⁹Department of Bionano Technology, Graduate School, Hanyang University, Seoul, 04763, Korea. Soojeong Shin, Daeyoung Han and Min Chul Park contributed equally to this work. Correspondence and requests for materials should be addressed to S.Kim. (email: sungkim@snu.ac.kr) or J.W.H. (email: jwh@hanyang.ac.kr)

pressurized environment^{7,8}. Alternative methods such as size exclusion chromatography^{9,10}, filtration¹¹, precipitation¹², and flow-cytometric analysis¹³ also suffer from their own limitations.

Miniaturized fluidic channel offers a potential means for experimental biological research^{14–16}, including exosome separation^{17–19}. Microfluidics builds upon various physicochemical parameters, such as chemical binding for antibody application^{20,21}, sieving²², acoustic wave²³, and field flow fractionation²⁴ onto micro- and nano-scale devices, which show high accuracy, precise control, lower energy consumption, and minimal sample size. Reported EV separating microdevices, however, have a narrow size range of sortable EVs, requiring additional pretreatment steps, which may cause sample dysfunction. Moreover, affinity-based EV separation catches only specific targets, thus missing unknown biological nanoparticles of potential value.

Here, we report noninvasive size-based EV separation on a chip and analyze separation patterns of micro- and nano-vesicles/particles. We used a microfluidic device to perform EV separation based on heterogeneous sizes with diameters between 0.1 and 5 μm . The suggested separation system requires less than an hour, with minimized external force, and can be an alternative method for EV evaluation (Fig. 1a). We applied various sizes of polystyrene (PS) particles as well as cell-cultured media containing different vesicles. Newly proceeded vesicle/particle separation methods as well as significant results on diagnosis were discussed.

Results

An effect of magnification ratio in microchannel for EV separation. The designed microchannel is depicted in Fig. 1b. The microdevice is composed of two inlets (Sample and Function channel), nine outlets, and a magnification channel that controls the overall flow pattern. Ideally, the Sample and Function flows come in contact inside the channel, then the pinched channel expands by 21 fold, allowing for spaces between vesicles/particles to increase perpendicular to the direction of the flow (Fig. 1c). The magnification channel draws part of the Function flow and any remaining Function and Sample flows are directed towards their respective outlets.

The vesicle/particle allocation could be altered as changing the ratio of flow withdrawn to overall inserted flow through the magnification channel, named as the magnification ratio ($\text{MR} [\%] = Q_M/Q_{\text{total}} \times 100$), where Q_M and Q_{total} are magnification flow rate and total flow rate, respectively. In the absence of magnification, meaning 0% MR, all Sample flow (red dye in Fig. 1e) ran to the first outlets and no significant change of colored outlet was observed until 50% MR was attained (Supplementary Fig. S2). When the MR increased to 70–90% under the 1:19 of Sample:Function ratio (Fig. 1e), the number of outlet channels containing Sample flow increased significantly. Additionally, effects of Sample:Function ratio and Q_{total} as well as MR were evaluated comprehensively. Yellowish areas at Fig. 1f represent partial loss of Sample flow withdrawn to the magnification channel rather than outlets #1 to #9, indicating over-magnification and commonly observed at $Q_{\text{total}} \geq 250 \mu\text{L}/\text{min}$ and high MR ($\geq 80\%$ at 1:9, $\geq 90\%$ at 1:19, $\geq 95\%$ at 1:99). Especially, the dye is spread more than the theoretically expected values (Table 1) when $Q_{\text{total}} > 200 \mu\text{L}/\text{min}$. On the other hand, dark blue areas at Fig. 1f indicate insufficient Sample flow broadening, which induce non-separated particle outflow. This kind of phenomena appeared when MR was lower than 60% at 1:9 and 80% at 1:19 when Q_{total} was fixed under $200 \mu\text{L}/\text{min}$. With the ratio of 1:99 of Sample:Function, MR is more than 80% for every Q_{total} condition. Based on these results, Q_{total} between 50–200 $\mu\text{L}/\text{min}$, MR between 60–90%, and 1:9 and 1:99 of Sample:Function ratios were set for the rest of the experiments.

Polystyrene (PS) rigid particle separation. PS microparticles of various sizes was chosen as model particles to confirm the separation ability of the designed microchannel. Figure 2 and Supplementary Fig. S3 explains how the MR regulates separation of micro-sized PS particles by changing outlet positions of particles. Applying magnification flow induced particles' shifting to the high-numbered outlets (Supplementary Fig. S3). Under the 70% MR, 1 μm particles were detected mostly at outlets #1 and #2, whereas 90% MR migrated the same size particles up to outlet #8 (Fig. 2). Upon reaching a 90% MR, amount of the 5 μm particles was dramatically reduced (Supplementary Fig. S4), which may infer the loss of particles through the magnification channel. Consequently, the MR regulates size-dependent particle separation by changing the outlet positions of particles.

Size-dependent separation of cell-derived EVs. The specific operating conditions, Sample:Function = 1:9, $Q_{\text{total}} = 200 \mu\text{L}/\text{min}$, MR = 75%, were applied on fabricated microchannel to separate biological vesicles. To prepare the EV mixture, SW620 cells were treated with low dose doxorubicin for 36 h (Supplementary Fig. S6). A low-speed centrifugation step removed cells, after which the supernatants were used as EVs-containing sample (Fig. 3a). Concentrated supernatant and buffer solution were introduced in Sample and Function channel, respectively. After separation proceeded, the suspensions collected from the nine outlets were analyzed by immunoblotting. Syntenin-1 and calreticulin were used as markers for exosomes and apoptotic bodies, respectively. Exosomes were detected at outlets #1 to #3, whereas apoptotic bodies were observed at outlets #5 to #9 (Fig. 3b and c). Additionally, the size of separated EVs was examined by transmission electron microscopy (TEM) analysis. Two representative outlets' samples (outlet 2: exosome, and outlet 8: apoptotic body) were analyzed by TEM, represented in Fig. 3. Outlet 2 samples showed exosomal cup-shaped morphology and size (30–100 nm), whereas outlet 8 samples showed aggregates including apoptotic bodies and larger sizes (500–2000 nm) (Fig. 3d and e). We confirmed down to 20 nm of biological particles under the electron microscope images of outlet #2 whereas no individual nanoparticles were detected at outlet #8. From the results, EVs appeared to be separated according to their size differences in our EV separation device.

Discussion

We designed a microfluidic chip for micro- and nano-particle separation including biological vesicles. The microchannel is composed of Sample and Function inlets, nine outlets, and a magnification channel which adjusts particle allocation by altering MR. Similar adaptation of magnification channel has been introduced^{25,26} for vesicles/particles to move further away from each other. In our case, magnification increased the separation efficiency of

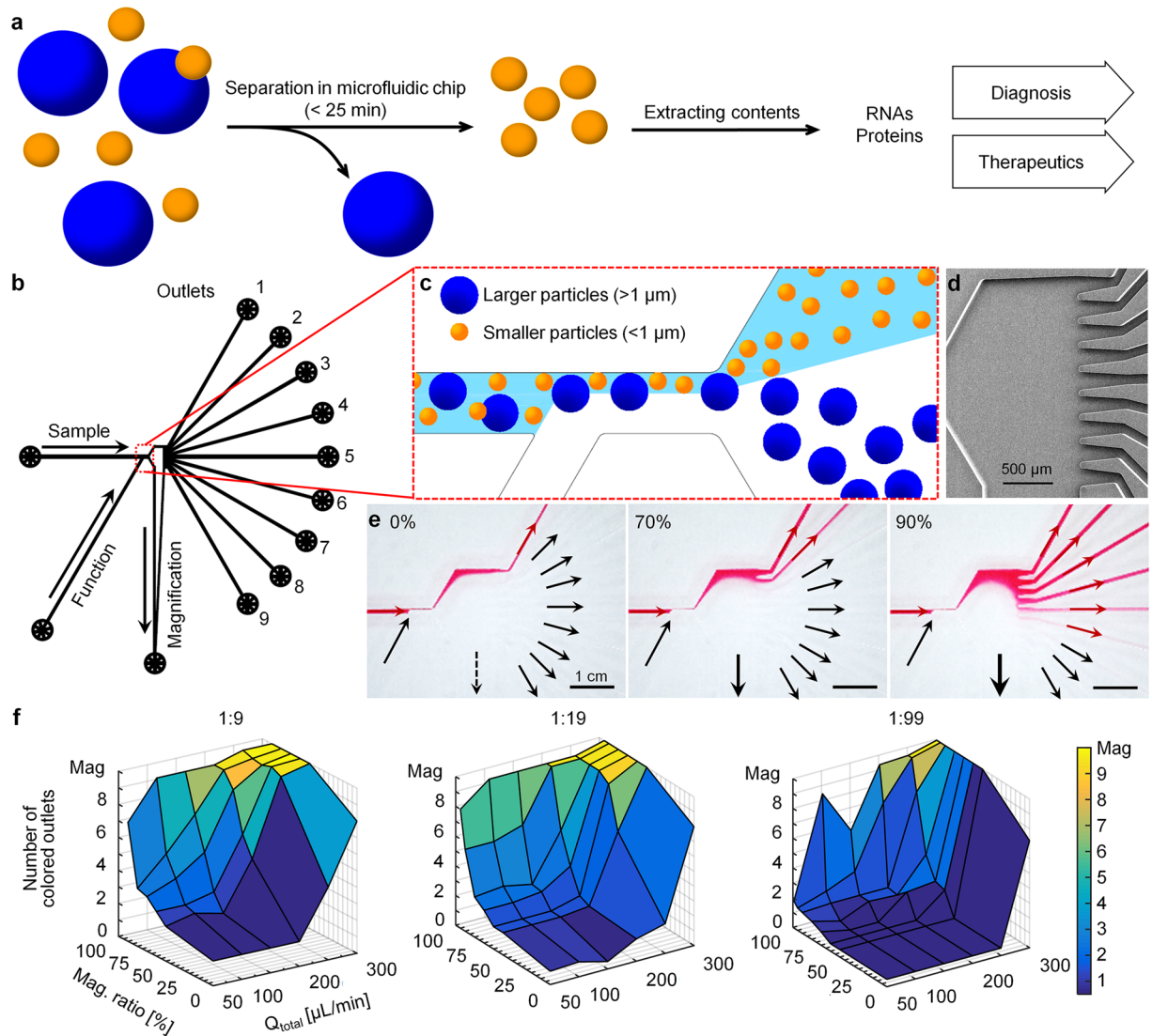


Figure 1. Microfluidic chip design and operational conditions. **(a)** Our goal is to separate unpurified biological nano-vesicles and/or micro-particles under mild external force. Since separated vesicles/particles are merely damaged during the process, the present methodologies and systems can be applied not only to diagnosis but also to therapeutics. **(b)** Microchannel design consisting of two inlets (Sample and Function channels), nine outlets (numbered from #1 to #9), and a magnification channel that withdraw the flow. **(c)** (Top view) Schematic diagram of size separation of nano-vesicles and micro-particles at the core region of microfluidic device (not to scale). Nano-vesicles and micro-particles are aligned through the upper wall. Then, larger vesicles/particles move toward outlets near the magnification channel while smaller ones travel to upper outlets when channel width is broadened. **(d)** Scanning electron microscopy (SEM) of the core part of the chip. **(e)** Pictures of sophisticated control of Sample flow from outlet channel 1 to 9 as a function of withdrawal speed: Under Sample:Function ratio is 1:19, 0, 70, and 90% of total flow is withdrawn to the magnification channel. Red dye represents Sample flow. Increased flow in withdrawing magnification channel results in spreading of Sample flow through outlet channels, #1 to #9. **(f)** Three-dimensional landscaped graphs depict relations among Q_{total} , magnification ratio (MR), and the number of outlets filled with Sample fluid under the different Sample:Function ratios, 1:9, 1:19, and 1:99. The spread area of Sample flow in the core part of the chip is increased as Q_{total} and MR increase.

vesicles/particles by draining Function flow through the magnification channel. This also minimizes sample dilution, a common feature of microfluidic separation system. We speculate that it should be possible to identify the outlets where particles of a specific size could be collected by controlling the MR. Unwanted or aggregated samples, whose size is larger than others, would be eliminated by flow withdrawal through the magnification channel.

Based on the purpose of the microfluidic separation explained above, determining optimal operational conditions was necessary. Three operation factors, Sample:Function, Q_{total} , and MR, were varied and the status of Sample fluid passing through the outlet channels was observed (Fig. 1e,f, Table 1, and Supplementary Fig. S2). Interestingly, high speed flow, $Q_{total} > 200 \mu\text{L}/\text{min}$, resulted in spreading of red dye inside all channels regardless

| Magnification ratio [%] | Number of colored outlets | | | | | | | | | | | | | | | | | | | | |
|-------------------------|---------------------------|-----|-----|-----------------------------|-----|-----|------------------------------|-----|-----|------------------------------|-----|-----|------------------------------|-----|-----|------------------------------|-----|-----|------------------------------|-----|-----|
| | theoretical | | | 50 $\mu\text{L}/\text{min}$ | | | 100 $\mu\text{L}/\text{min}$ | | | 150 $\mu\text{L}/\text{min}$ | | | 200 $\mu\text{L}/\text{min}$ | | | 250 $\mu\text{L}/\text{min}$ | | | 300 $\mu\text{L}/\text{min}$ | | |
| | A* | B* | C* | A | B | C | A | B | C | A | B | C | A | B | C | A | B | C | A | B | C |
| 0 | 0.9 | 0.5 | 0.1 | 1.5 | 0.9 | 0.5 | 1.5 | 1.0 | 0.5 | 1.5 | 0.5 | 0.5 | 1.5 | 1.5 | 0.5 | 4.4 | 2.0 | 0.5 | 8.0 | 8.0 | 7.2 |
| 50 | 1.8 | 0.9 | 0.2 | 2.1 | 1.5 | 0.5 | 2.5 | 1.5 | 0.5 | 2.1 | 1.5 | 0.5 | 5.0 | 1.7 | 0.5 | 9.6 | 6.2 | 0.5 | 10 | 10 | 10 |
| 60 | 2.3 | 1.1 | 0.2 | 2.7 | 1.5 | 0.5 | 2.7 | 1.5 | 0.5 | 3.1 | 1.5 | 0.5 | 6.2 | 2.0 | 0.5 | 9.9 | 9.0 | 2.0 | 10 | 10 | 10 |
| 70 | 3.0 | 1.5 | 0.3 | 3.3 | 2.2 | 0.9 | 4.0 | 2.2 | 0.5 | 5.2 | 2.4 | 0.5 | 8.6 | 3.6 | 2.0 | 9.7 | 9.5 | 2.2 | 10 | 10 | 10 |
| 80 | 4.5 | 2.3 | 0.5 | 3.5 | 2.7 | 1.2 | 5.2 | 2.9 | 0.7 | 7.2 | 2.5 | 1.5 | 9.5 | 5.6 | 1.4 | 9.8 | 9.5 | 3.6 | 10 | 10 | 10 |
| 90 | 9.0 | 4.5 | 0.9 | 7.2 | 5.5 | 1.4 | 9.5 | 5.5 | 1.5 | 9.5 | 6.1 | 1.5 | 9.5 | 9.5 | 1.5 | 10 | 9.5 | 7.4 | 10 | 10 | 10 |
| 95 | | 9.0 | 1.8 | | 8.0 | 1.5 | | 9.5 | 2.1 | | 9.5 | 2.9 | | 9.5 | 7.0 | | 9.5 | 9.5 | | 10 | 10 |
| 99 | | | 9.0 | | | 1.8 | | | 8.5 | | | 5.5 | | | 9.4 | | | 9.5 | | | 10 |

Table 1. Number of colored outlets according to the magnification ratio (MR), Q_{total} , and Sample:Function ratios. *Sample:Function ratio (A) 1:9, (B) 1:19, (C) 1:99.

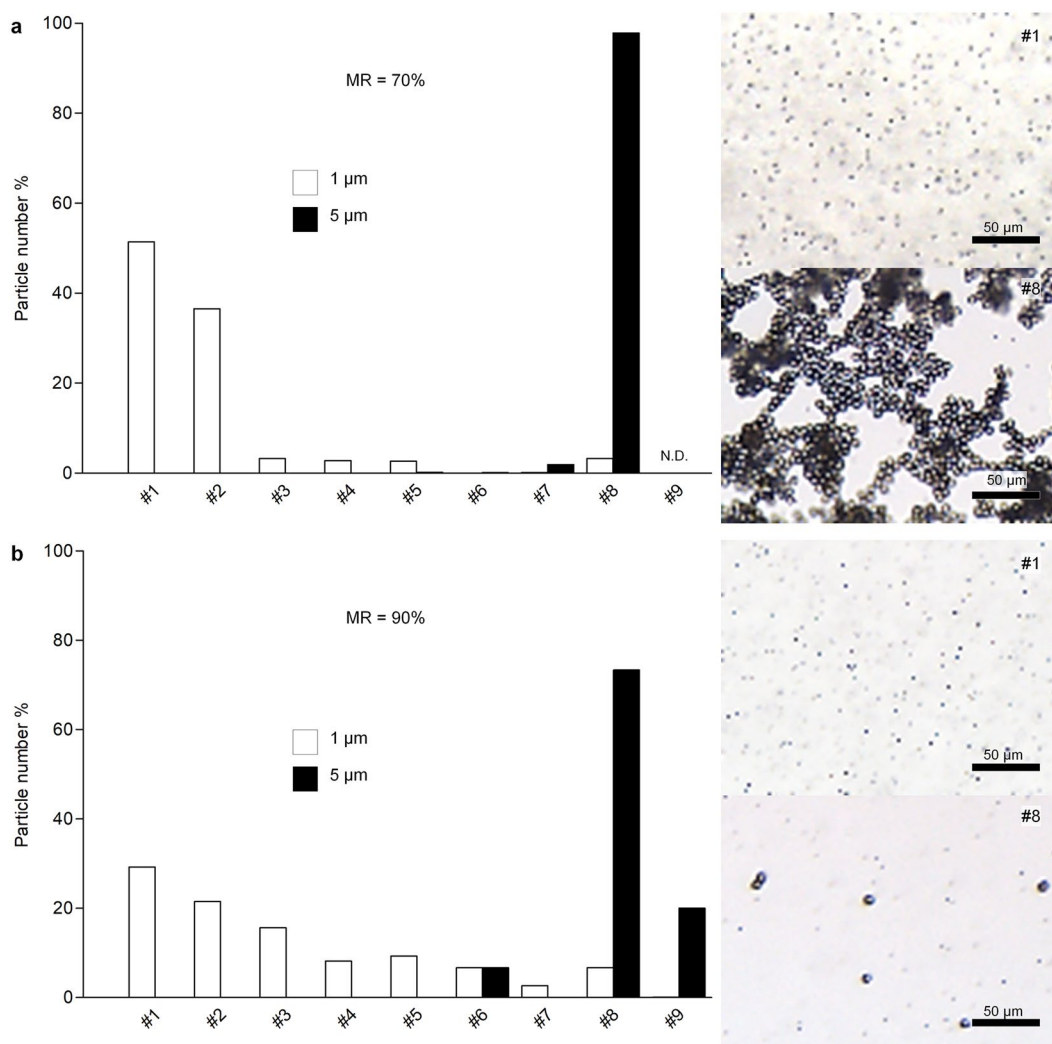


Figure 2. Effect of magnification on particle separation. Mixture of 1 and 5 μm PS microparticles were separated under different magnification ratio (MR), (a) 70% (b) 90%. Most of the 5 μm particles are collected at #8 outlet at (a) and clearly sorted from 1 μm particles. (b) On increasing MR up to 90%, 1 μm particles shift to the high-numbered outlets. More magnification not only spread smaller particles toward more outlets but also moved most of bigger particles moved over the #8 outlet. N.D. represents ‘not detected’.

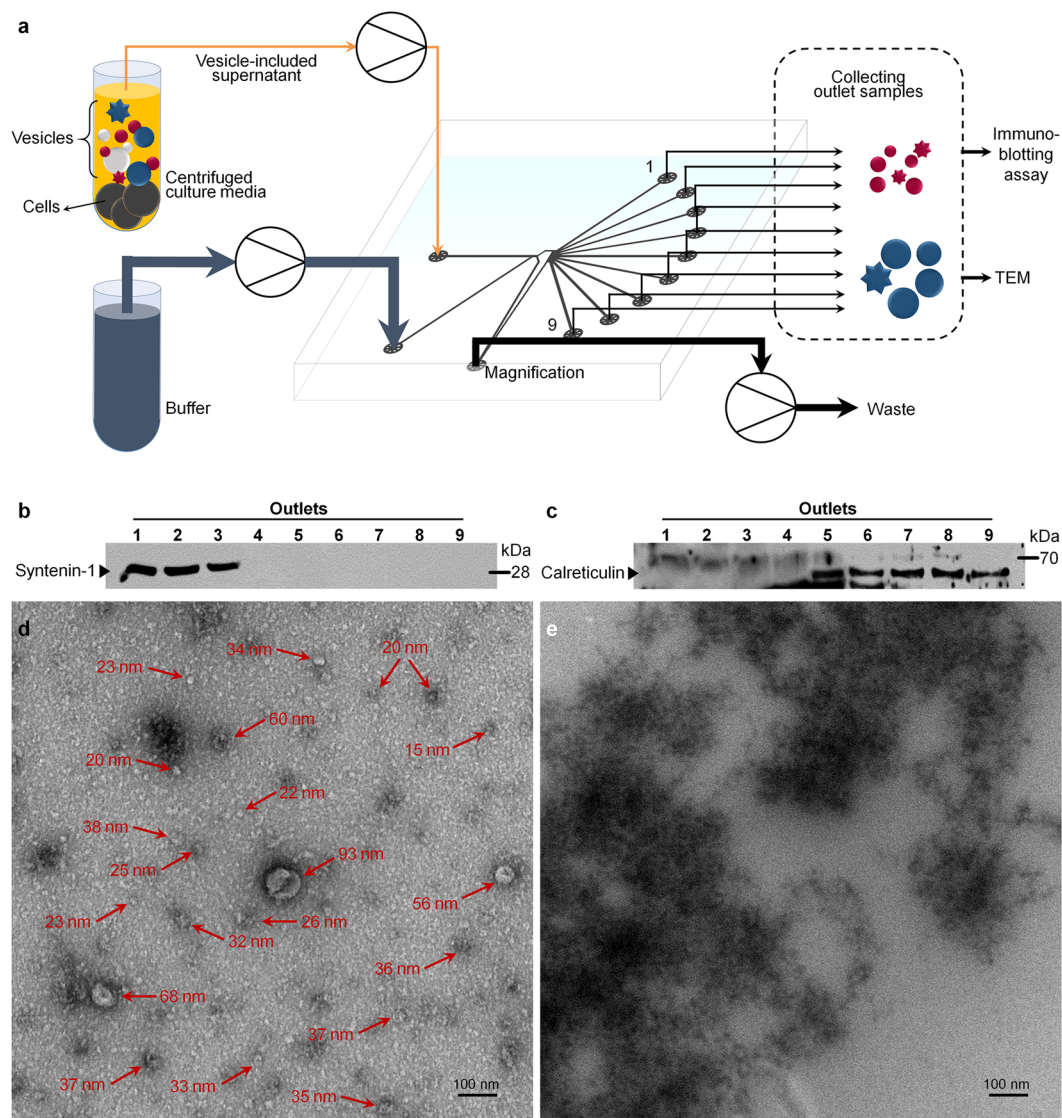


Figure 3. Separation of nanometer- and/or micrometer- biological vesicles from cell culture. **(a)** Separation procedures. After mild centrifugation, cells are discarded and only vesicle-suspended media is concentrated. The enriched vesicles and buffer are separately introduced to Sample and Function channels, respectively. Samples from each outlet are collected and analyzed by immunoblotting assay and TEM. **(b) (c)** Immunoblotting results from the separated vesicles with 75% MR are shown as cropped images from full-length western blots. Syntenin-1 and calreticulin antibodies were used as markers for 50–200 nm ranged vesicles, exosomes, and 1–5 μm of apoptotic bodies, respectively. Exosomes are clearly separated through channel #1 to #3. On the other hand, larger microvesicles including apoptotic bodies are collected outlets #5 to #9. **(d) (e)** Transmission electron microscopy (TEM) images of vesicles collected from different outlets: **(d)** exosomes at outlet #2 show a distinct cup-shape, which is a specific characteristic of exosomes. Additional vesicles sized down to 20 nm are also detected. Enlarged picture of **(d)** is shown in Supplementary Fig. S7. **(e)** Apoptotic body included aggregates from outlet #8. Round-shape vesicles (arrows at **(d)**) are present in outlet #2 fraction but not shown in outlet #8 fraction, indicating nanometer-sized biological particles were successfully separated from the micron particles including apoptotic bodies.

of Sample:Function ratio (Supplementary Fig. S2), resulting in larger numbers of colored outlets than the theoretically expected values (Table 1). The turbulence may be generated from the Sample-Function joining region causing dilution of Sample fluid and a considerable amount of sample being lost to the magnification channel. Thus, we determined the maximum flow rate to be 200 $\mu\text{L}/\text{min}$.

The sorting behavior of PS microparticles on the present microchannel was similar to conventional pinched-flow fractionation, but was not confirmed for nanoparticles. In previous reports, synthetic particles smaller than 1 μm had been hard to separate²⁷ due to resolution degrading by Brownian motion. However, the flow rate in our system was relatively higher than previously reported ones, allowing us to neglect the diffusion effect. One-dimensional diffusion distance when passing through the channels was calculated as follows:

$\langle d^2 \rangle = kT \times t / 3\pi\eta R$, where $\langle d^2 \rangle$, k , T , η , R , and t represent mean-square displacement, Boltzmann constant, temperature, dynamic viscosity, particle radius, and diffusion time, respectively. Calculated results were <0.20 and $<1.3 \mu\text{m}$, less than 0.2% of the channel widths of pinched and broadened regions, respectively. Instead, our system had a relatively large Reynolds number, which was calculated using the equation: $\text{Re} = (\text{Inertial force}) / (\text{Viscous force}) = \rho D_H v / \eta = 2\rho Q / \eta(h+w)$, where ρ , D_H , v , η , Q , h , w represent fluid density, hydraulic diameter of the microchannel (for a rectangular channel, $D_H = 2hw/(h+w)$), flow velocity, dynamic viscosity, volumetric flow rate, channel height, and channel width, respectively. The calculated Reynolds numbers for the pinched and broadened region were 27–54 and 1.8–3.5, respectively. This finding implied that flow inside the microchannel was distinguished from the conventional Stokes flow ($\text{Re} \ll 1$) usually observed in microfluidics. Our microfluidic system managed to maintain a laminar flow with Reynolds numbers less than 2100; however, inertial force could not be ignored for microparticles²⁸. Inertia may affect nanoparticle separation. Nevertheless, maintaining a high flow rate ($Q_{\text{total}} > 100 \mu\text{L}/\text{min}$) improves particle separation speed, indicating the ability of the microfluidic device to treat large sample volume.

EVs, especially exosomes, have been developed as markers in diagnostics and therapeutics. Unfortunately, although EVs are good candidates for pharmaceutical development, isolation methods are limited and have limitations. For example, immuno-precipitation methods isolate only specific marker-expressing EVs. Ultracentrifugation methods have a low degree of resolution for size-dependent separation and induce damage in the EVs. Compared with conventional EV isolation methods, our microfluidic-based EV separation system offers fine-tuned EV separation in a size-dependent manner since apoptotic bodies (1–5 μm) were much larger than exosomes (hydrodynamic diameter, 50–200 nm)^{4,29}, and is a flexible platform for targeting different sized EVs. As shown in Supplementary Fig. S5, the size-separation tendency of vesicles was similar to that in the PS particle separation. Even though the particle properties would be different, we confirmed that the vesicle/particle mixtures, whose sizes were approximately 1 μm , could be separated using our system. Moreover, MR is adjusted depending on what kind of target is chosen. We applied distinct dissimilar operational conditions; however, both biological vesicle and PS particles having different size ranges were successfully separated. Since this platform suggests that differently characterized EVs can be isolated, new diagnostic markers and therapeutic candidates could be identified using this platform.

Based on the results above, the suggested separation method covers wide range of biological nanoparticle. Microparticles should be separated under $\text{MR} < 70\%$ to protect loss of samples through the magnification channel (Fig. 2). Under the same condition of PS particle separation, the number of colored outlets was 2.2. In case of EV separation from the cultured media (Fig. 3), most of biological vesicles have sub-micron sized diameter, which is much smaller than tested PS particles, thus we adapted the condition whose number of colored outlets was approximately 9.0. From this compared results, we propose that the operational conditions of higher number of colored outlets should be set for smaller vesicle/particle separation. Consequently, vesicle/particle of various sizes, from sub-micron to tens of micron in diameter, could be sorted in single microchannel by controlling MR only. In common, sample pretreatment has been accompanied in order to remove aggregated impurities that block the channel and fail the chip operation. Our suggesting microchannel can eliminate pretreatment step by discarding larger impurities such as cells and aggregated vesicles through magnification channel as well as separate specific size particles through nine outlets simultaneously.

In summary, noninvasive microfluidic particle separation was performed to separate micro- and nano-particles by size, and eventually separate extracellular vesicles. This microchip contains a magnification channel; hence, particle allocation inside the channel and/or toward the outlets is controllable according to the characteristics of sample fluid and contained particles through MR change. We successfully separated nanometer-sized exosomes and apoptotic bodies at outlets #1 to #3 and outlets #5 to #9, respectively. Biological differences of the vesicles were confirmed by immunoblotting assay and TEM image.

The present system and methodology provided new ways of biological nanovesicle separation in microfluidic formats especially Reynolds number ranging in 1 to 100 minimizing diffusion effects. Efforts to understand specific positioning of vesicles or particles in the micro channels should be continued. In the meantime, separation of particles under increased operation speeds could enhance the separation efficiencies. Indeed, we expect that the separation of nano- to micro-sized particles and vesicles from biological samples including blood without any pretreatments based on the present results have great potentials to contribute in the advancement of biological pharmaceutical and diagnostic sciences.

Methods

Microchannel design and microchip fabrication. The PDMS-based microchannel was prepared following previously reported methods^{14,30}. The microchannel was designed using AutoCAD (Autodesk Inc., San Rafael, CA) and printed as a 25,000 dpi photomask (Microtech, Korea). After spin-coating and baking the SU-8 photoresist (Microchem, Westborough, MA) on a 4 in silicon wafer, the photomask was placed, UV-exposed, and developed. Next, PDMS (Sylgard 184[®], Dow Corning, MI) was mixed with the elastomer at a ratio of 10:1, poured over the SU-8 microchannel mold, and cured for 40 min at 80 °C in the oven. All inlets and outlets on the PDMS chip were punched using a micro-puncher (Syneo, Angleton, TX). PDMS, whose mixing ratio with the elastomer was 20:1, was spin-coated on a clean glass slide with a thickness of 10–20 μm , followed by curing for 20 min at 80 °C. The punched PDMS chip was then placed on the partially cured PDMS coated glass slide and curing was applied for a further 18 h.

Preparation of PS particle suspension and biosamples. Polystyrene (PS) microparticles and nanoparticles were purchased from Sigma (St. Louis, MO). The mixing concentrations of the PS particles were 0.1% (w/w) for 1 μm and 0.9% (w/w) for 5 μm particles. All solutions were suspended in distilled water and mixed immediately prior to beginning the experiment. The apoptotic bodies were prepared by incubating SW620 (ATCC,

Manassas, VA) cells with 2 μM doxorubicin (Sigma-Aldrich, St. Louis, MO) in RPMI-1640 medium containing 1% penicillin-streptomycin (Hyclone, Logan, UT) for 36 h. The culture medium was harvested and cells were removed by centrifugation at 400 g for 10 min. The supernatant was centrifuged at 2,000 g for 20 min and the pellet was resuspended in PBS for the experiment. Exosome was also obtained from SW620 cell culture media without doxorubicin. After cells and cell debris removal by centrifugation, the supernatant was centrifuged additionally at 10,000 g for 20 min. The supernatant were concentrated with 50 K Amicon centrifugal filters (Millipore, Billerica, MA) for harvest exosomes. Details are explained in Supplementary Fig. S6.

Experimental operating conditions. Three syringe pumps (Fusion 100 and 200, Chemyx, Stafford, TX) were used to generate the microflow; one for infusion of vesicle/particle suspended sample, one for infusion of Dulbecco's phosphate buffered saline (DPBS, Welgene, Republic of Korea)- based Function flow, one for withdrawal flow from the magnification channel. Q_{total} was adjusted to 200 $\mu\text{L}/\text{min}$ (for biological sample separation, MR = 75%) and 100 $\mu\text{L}/\text{min}$ (for PS particle separation, various MR applied). The input ratios of Sample:Function of biological samples' and PS particles' separation were 20:180 and 5:95, respectively. Tygon Microbore tubings (Cole-Parmer, Vernon Hills, IL) connected syringes to micropins (New England Small Tube, Litchfield, NH), which were fit to the punched holes. The ends of the connected tubing were dipped in distilled water and the water level was adjusted to that at the surface, to allow for sampling from the outlets and render negligible the effect of pressure differences at the outlets. Distilled water was applied to flush air bubbles from inside the channel, following which particle separation could proceed.

Calculation of the theoretical value of Number of colored outlets. To compare the flow pattern of Sample fluid (red dye) on Fig. 1e and Supplementary Fig. S2, theoretically expected values of Number of colored outlets were calculated. Assuming no mixing between the Sample and Function fluid, it is expected that only Function flow is withdrawn through the magnification channel when Function flow rate is similar to or higher than Magnification flow rate ($Q_F \geq Q_M$). We assumed that the remained fluid is distributed evenly to the 9 outlets, thus $(Q_{total} - Q_M)/N = Q_S/N_{colored}$ where Q_{total} , Q_S , N , and $N_{colored}$ are total flow rate, Sample flow rate, total outlet numbers (fixed as 9 in the present work), and Number of colored outlets, respectively. MR (Magnification ratio) [%] = $100Q_M/Q_{total}$ thus, Number of colored outlets can be derived as follow:

$$N_{colored} = \frac{NQ_S}{(Q_{total} - Q_M)} = \frac{100NQ_S}{Q_{total}(100 - MR)}$$

Under the 1:19 Sample:Function ratio with $Q_{total} = 100 \mu\text{L}/\text{min}$ and MR = 80%, $Q_S = 5 \mu\text{L}/\text{min}$, thus, $N_{colored} = 2.25$. The calculated values for every condition are summarized in Table 1.

Analysis of outlet samples. The samples were collected in nine tubes and magnification syringe, and were analyzed by several methods (the flowchart for the overall procedure is presented in Supplementary Fig. S1). For micro-sized PS particles, the separated and collected samples were placed in a 96-well plate, and the number of particles was counted using an optical microscope. For biological vesicles, exosomes and apoptotic bodies were distinguished by immunoblotting assay. Proteins and EVs were precipitated from outlet samples using trichloroacetic acid (TCA, Sigma-Aldrich, St. Louis, MO). After neutralization with 100 mM HEPES (pH 8.0), precipitates were loaded on SDS-PAGE and transferred to PVDF membrane (Millipore, Billerica, MA) for immunoblotting. Antibodies against syntenin-1 (Santa Cruz, Dallas, TX) and calreticulin (Thermo Scientific, Lafayette, CO) were used to probe for exosomes and apoptotic bodies, respectively. These vesicles were confirmed by electron microscopy imaging. Isolated nanoparticles were diluted 5 fold in PBS, then 5 μL of the sample solution was immediately (~ 5 sec) applied to a carbon-coated grid that had been glow-discharged (Harrick Plasma) for 3 min in air, and the grid was negatively stained using 1% uranyl acetate. The same procedure was used for all negatively stained specimens. The stained vesicles were imaged under a Hitachi H-7600 (Hitachi, Tokyo, Japan) transmission electron microscope at 80 kV.

Mean particle size calculation of each sample. As explained in Supplementary Fig. S1, all analyzed data were re-calculated to determine the mean particle size of each outlet sample and to identify the separation profiles (Figs 2 and 3, and Supplementary Fig. S3). For PS microparticle size calculation, the following equation was used: (Mean particle size) = $D_a p_a + D_b p_b / (p_a + p_b)$, where D_i and p_i are particle diameter and particle number percentage of 'i' μm particles ($i = 1, 5, 10$), respectively. For example, if the number of 1 μm particle is 10 times higher than 5 μm particles, mean particle size is calculated to be 1.36 μm . For biological vesicles, vesicle types and expected particle size range were confirmed from the immunoblotting data and the size-represented reference⁶, respectively. To compare the separation tendencies shown in Supplementary Fig. S5b, larger size position at y-axis was decided for apoptotic body.

References

1. Fuhrmann, G., Herrmann, I. K. & Stevens, M. M. Cell-derived vesicles for drug therapy and diagnostics: Opportunities and challenges. *Nano Today* **10**, 397–409 (2015).
2. Tominaga, N., Yoshioka, Y. & Ochiya, T. A novel platform for cancer therapy using extracellular vesicles. *Adv. Drug Delivery Rev.* **95**, 50–55 (2015).
3. Ohno, S.-I. *et al.* Systemically Injected Exosomes Targeted to EGFR Deliver Antitumor MicroRNA to Breast Cancer Cells. *Mol. Ther.* **21**, 185–191 (2013).
4. van der Pol, E., Böing, A. N., Harrison, P., Sturk, A. & Nieuwland, R. Classification, functions, and clinical relevance of extracellular vesicles. *Pharmacol. Rev.* **64**, 676–705 (2012).
5. Batrakova, E. V. & Kim, M. S. Using exosomes, naturally-equipped nanocarriers, for drug delivery. *J. Control. Release* **219**, 396–405 (2015).

6. Colombo, M., Raposo, G. & Thery, C. Biogenesis, secretion, and intercellular interactions of exosomes and other extracellular vesicles. *Annu. Rev. Cell Dev. Biol.* **30**, 255–289 (2014).
7. Rood, I. M. *et al.* Comparison of three methods for isolation of urinary microvesicles to identify biomarkers of nephrotic syndrome. *Kidney Int.* **78**, 810–816 (2010).
8. Tauro, B. J. *et al.* Comparison of ultracentrifugation, density gradient separation, and immunoaffinity capture methods for isolating human colon cancer cell line LIM1863-derived exosomes. *Methods* **56**, 293–304 (2012).
9. Merchant, M. L. *et al.* Microfiltration isolation of human urinary exosomes for characterization by MS. *Proteom. Clin. Appl.* **4**, 84–96 (2010).
10. Nordin, J. Z. *et al.* Ultrafiltration with size-exclusion liquid chromatography for high yield isolation of extracellular vesicles preserving intact biophysical and functional properties. *Nanomed.-Nanotechnol.* **11**, 879–883 (2015).
11. Heinemann, M. L. *et al.* Benchtop isolation and characterization of functional exosomes by sequential filtration. *J. Chromatogr. A* **1371**, 125–135 (2014).
12. Paolini, L. *et al.* Residual matrix from different separation techniques impacts exosome biological activity. *Sci. Rep.* **6**, 23550 (2016).
13. Dragovic, R. A. *et al.* Isolation of syncytiotrophoblast microvesicles and exosomes and their characterisation by multicolour flow cytometry and fluorescence Nanoparticle Tracking Analysis. *Methods* **87**, 64–74 (2015).
14. Shin, S., Yoo, Y. J. & Hong, J. W. Microgravity separation of alginate empty capsules from encapsulated pancreatic islets using a microfluidic system. *J. Nanosci. Nanotechnol.* **15**, 7876–7880 (2015).
15. Hamon, M. & Hong, J. W. New tools and new biology: recent miniaturized systems for molecular and cellular biology. *Mol. Cells* **36**, 485–506 (2013).
16. Dai, J. *et al.* Charting microbial phenotypes in multiplex nanoliter batch bioreactors. *Anal. Chem.* **85**, 5892–5899 (2013).
17. Liga, A., Vliegthart, A. D. B., Oosthuizen, W., Dear, J. W. & Kersaudy-Kerhoas, M. Exosome isolation: A microfluidic road-map. *Lab Chip* **15**, 2388–2394 (2015).
18. Santana, S. M., Antonyak, M. A., Cerione, R. A. & Kirby, B. J. Microfluidic isolation of cancer-cell-derived microvesicles from heterogeneous extracellular shed vesicle populations. *Biomed. Microdevices* **16**, 869–877 (2014).
19. Wunsch, B. H. *et al.* Nanoscale lateral displacement arrays for the separation of exosomes and colloids down to 20 nm. *Nat. Nanotechnol.* **11**, 936–940 (2016).
20. Dudani, J. S. *et al.* Rapid inertial solution exchange for enrichment and flow cytometric detection of microvesicles. *Biomicrofluidics* **9**, 014112 (2015).
21. Kanwar, S. S., Dunlay, C. J., Simeone, D. M. & Nagrath, S. Microfluidic device (ExoChip) for on-chip isolation, quantification and characterization of circulating exosomes. *Lab Chip* **14**, 1891–1900 (2014).
22. Davies, R. T. *et al.* Microfluidic filtration system to isolate extracellular vesicles from blood. *Lab Chip* **12**, 5202–5210 (2012).
23. Lee, K., Shao, H., Weissleder, R. & Lee, H. Acoustic purification of extracellular microvesicles. *ACS Nano* **9**, 2321–2327 (2015).
24. Sitar, S. *et al.* Size characterization and quantification of exosomes by asymmetrical-flow field-flow fractionation. *Anal. Chem.* **87**, 9225–9233 (2015).
25. Nho, H. W. & Yoon, T. H. Enhanced separation of colloidal particles in an AsPFF device with a tilted sidewall and vertical focusing channels (t-AsPFF-v). *Lab Chip* **13**, 773–776 (2013).
26. Srivastav, A., Podgorski, T. & Couplier, G. Efficiency of size-dependent particle separation by pinched flow fractionation. *Microfluid. Nanofluid.* **13**, 697–701 (2012).
27. Dou, H., Lee, Y. J., Jung, E. C., Lee, B. C. & Lee, S. Study on steric transition in asymmetrical flow field-flow fractionation and application to characterization of high-energy material. *J. Chromatogr. A* **1304**, 211–219 (2013).
28. Bhagat, A. A., Hou, H. W., Li, L. D., Lim, C. T. & Han, J. Pinched flow coupled shear-modulated inertial microfluidics for high-throughput rare blood cell separation. *Lab Chip* **11**, 1870–1878 (2011).
29. Chernyshev, V. *et al.* Size and shape characterization of hydrated and desiccated exosomes. *Anal. Bioanal. Chem.* **407**, 3285–3301 (2015).
30. Kim, D. *et al.* Quantitative analysis of pneumatically driven biomimetic micro peristalsis. *Sci. Adv. Mat.* **6**, 2428–2434 (2014).

Acknowledgements

This research was supported by the Global Frontier Project Grant (NRF-2014M3A6A4062860, NRF-2013M3A6A4046061, NRF-M3A6A4-2010-0029785), Small Grant Exploratory Research (NRF-2014R1A1A2A160552910) and Engineering Research Center (2008-0061891) of the National Research Foundation, funded by the Ministry of Science, ICT & Future Planning of Korea.

Author Contributions

S.S., D.H., M.C.P., S.K., and J.W.H. conceived the concept; S.S., D.H., M.C.P., and J.W.H. designed experiments and wrote the manuscript; D.H. and M.C.P. executed EV sample preparation; S.S. designed and fabricated EV separation chip; S.S. and D.H. operated EV separation chip; D.H., M.C.P., J.Y.M. analyzed separated EVs using immunoblotting assay and TEM imaging; S.S., D.H., M.C.P., J.Y.M., J.C., H.C., S.K., J.W.H. discussed results and commented on the manuscript.

Additional Information

Supplementary information accompanies this paper at doi:10.1038/s41598-017-08826-w

Competing Interests: The authors declare that they have no competing interests.

Publisher's note: Springer Nature remains neutral with regard to jurisdictional claims in published maps and institutional affiliations.



Open Access This article is licensed under a Creative Commons Attribution 4.0 International License, which permits use, sharing, adaptation, distribution and reproduction in any medium or format, as long as you give appropriate credit to the original author(s) and the source, provide a link to the Creative Commons license, and indicate if changes were made. The images or other third party material in this article are included in the article's Creative Commons license, unless indicated otherwise in a credit line to the material. If material is not included in the article's Creative Commons license and your intended use is not permitted by statutory regulation or exceeds the permitted use, you will need to obtain permission directly from the copyright holder. To view a copy of this license, visit <http://creativecommons.org/licenses/by/4.0/>.